

NANOTECHNOLOGICAL EVALUATION OF VOLCANIC CLAYS WITH APPLICATION IN BITUMEN IMPROVEMENT

Ignacio Bladimir Cerón Guerra, María José Cerón, Luis Guillermo Loría, Marcelo Salvador, Cristian Lemos and Giovanni Sáenz-Arce

SUMMARY

Clays are raw materials for modern industry and today they are even used for medicines. In an area of 4000 km², the San Tadeo geological formation, Ecuador, has a nano clay deposit arranged in six levels (A1 to A6). Physicochemical studies of field samples showed the presence of more than 60% of aluminosilicates in the upper levels A1, A2. Laser granulometry found an average particle size of 30 to 250nm. Nitrogen adsorption-desorption isotherm determined the average specific surface area of 280.3m²/g. IFTR, XRF, SPECMIN-TSG showed the spectra with the presence of vermiculite, allophane and bentonite minerals. With TGA/DCS a mass loss of up to 42.5% was observed for clays A1, A2, A3, at the final calcination temperature of 1000°C, with endothermic and exothermic manifesta-

tions. High adsorption capacity was found for A1 and A2 clays over 30% in their order, and over the other geological horizons; the property was activated when the clay was calcined in the temperature window of 250 to 300°C. EDS, energy dispersive spectroscopy found the presence of Si and Al in the sample of bitumen mixture enhanced with additive A1. SEM confirmed the presence of exfoliated and dispersed A1 additive in the enhanced bitumen mix prepared with 3% by weight of active agent. With DSR (T= 70°C operational) the complex modulus G* = 2326pa (640pa original) and δ = -8.7° points (85° original) were measured, with an improvement of 363%. The new material is applicable as road pavement in medium and high ambient temperature areas due to its higher stiffness.

Introduction

A clay has been defined as a material mainly made up of fine-grained minerals

corresponding to clay minerals, looks like a material of plastic condition when properly wetted and becomes hard when dehydrated or calcined (Bergaya *et*

al., 2006). Clays are mainly made up of phyllosilicates (Brigatti and Galan, 2024). Today's industry uses this material in many applications, and it

is of great interest to the scientific community (Punia Bangar *et al.*, 2023).

The classification of clay minerals is of three types

KEYWORDS / Adsorption / Bitumen / Clay / Nanometric Properties / Rigidity /

Received: 04/15/2024. Modified: 06/04/2024. Accepted: 06/06/2024.

Ignacio Bladimir Cerón Guerra (Corresponding author). Master in Petroleum Exploration and Exploitation, IFP Energies Nouvelles (IFPEN), France. Doctorate in Natural Sciences for Development (DOCINADE), Instituto Tecnológico de Costa Rica, Universidad Nacional de Costa Rica and Universidad Estatal a Distancia, Costa Rica. Consultant and Researcher, Senescyt, Quito. Address: e-mail: ivcgoill@gmail.com. ORCID: <https://orcid.org/0000-0002-6373-9772>.

María José Cerón. Petroleum Engineer, Escuela Politécnica Nacional, Quito, Ecuador. Senior Reservoir Development Engineer, Latin America Latam, Schlumberger International, Quito, Ecuador. e-mail: maria.ceron1998@gmail.com. ORCID: <https://orcid.org/0000-0002-5665-8755>.

Luis Guillermo Loría. PhD. in Civil Engineering, University of Nevada, Reno, United States. Vice Chancellor of UIN Research, Universidad Isaac Newton, San José, Costa Rica. President of the International Society of Asphalt

Pavements (ISAP). e-mail: lloria@uin.cr. ORCID: <https://orcid.org/0000-0002-2336-9703>.

Marcelo Salvador. MSc in Crude Oil and Derivates Transportation System. Escuela Politécnica Nacional, Quito Ecuador. Professor, Escuela Politécnica Nacional, Quito, Ecuador. e-mail: marcelo.salvadorq@epn.edu.ec. ORCID: <https://orcid.org/0000-0003-4613-3311>.

Cristian Lemos. MSc in Construction of Onshore and Offshore Horizontal and Multi-lateral Wells, Gubkin Russian State University of Oil and

Gas, Moscow, Russia. General Manager, International Business, Quito, Ecuador. e-mail: bryanlemos94@hotmail.com. ORCID: <https://orcid.org/0000-0003-1848-7980>.

Giovanni Sáenz-Arce. PhD in Nanoscience and Nanotechnology, Universidad de Alicante, Alicante, Spain. Director and Researcher, Universidad Nacional de Costa Rica, Costa Rica and Universidad de Murcia, Spain. e-mail: giovanni.saenz.arce@una.ac.cr. ORCID: <https://orcid.org/0000-0003-1848-7980>.

EVALUACIÓN NANOTECNOLÓGICA DE ARCILLAS VOLCÁNICAS CON APLICACIÓN EN LA MEJORA DEL ASFALTO

Ignacio Bladimir Cerón Guerra, María José Cerón, Luis Guillermo Loría, Marcelo Salvador, Cristian Lemos y Giovanni Sáenz-Arce

RESUMEN

Las arcillas son materias primas para la industria moderna y hoy se utilizan incluso para medicamentos. En una superficie de 4.000 km², la formación geológica de San Tadeo, en Ecuador, presenta un yacimiento de nanoarcillas dispuestas en seis niveles (A1 a A6). Estudios físico-químicos de muestras de campo mostraron la presencia de más del 60% de aluminosilicatos en los niveles superiores A1, A2. La granulometría láser encontró un tamaño medio de partícula de 30 a 250nm. La isoterma de adsorción-desorción de nitrógeno determinó una superficie específica media de 280,38m²/g. IFTR, XRF, SPECMIN-TSG mostraron los espectros con la presencia de minerales de vermiculita, alófano y bentonita. Con TGA/DCS se observó una pérdida de masa de hasta el 42,5% para las arcillas A1, A2, A3, a la temperatura final de calcinación de 1000°C, con manifestacio-

nes endotérmicas y exotérmicas. Se encontró una alta capacidad de adsorción para las arcillas A1 y A2 por encima del 30% en su orden, y por encima de los otros estratos geológicos; la propiedad se activó cuando la arcilla se calcinó en la ventana de temperatura de 250 a 300°C. La espectroscopia de dispersión de energía (EDS) constató la presencia de Si y Al en la muestra de mezcla bituminosa mejorada con el aditivo A1. El SEM confirmó la presencia de aditivo A1 exfoliado y disperso en la mezcla de betún mejorado preparada con un 3% en peso de agente activo. Con DSR (T= 70°C operacional) se midió el módulo complejo $G^* = 2326\text{pa}$ (640pa original) y $\delta = -8,7^\circ$ puntos (84° original), con una mejora del 363%. El nuevo material es aplicable como pavimento de carreteras en zonas de temperatura ambiente media y alta debido a su mayor rigidez.

VALIAÇÃO NANOTECNOLÓGICA DE ARGILAS VULCÂNICAS COM APLICAÇÃO NO APRIMORAMENTO DO BETUME

Ignacio Bladimir Cerón Guerra, María José Cerón, Luis Guillermo Loría, Marcelo Salvador, Cristian Lemos e Giovanni Sáenz-Arce

RESUMO

As argilas são matérias-primas para a indústria moderna e, atualmente, são usadas até mesmo em medicamentos. A formação geológica de San Tadeo, no Equador, que abrange uma área de 4.000 km², contém um depósito de nanoclásios dispostos em seis níveis (A1 a A6). Estudos físico-químicos de amostras de campo mostraram a presença de mais de 60% de aluminossilicatos nos níveis superiores A1 e A2. A granulometria a laser encontrou um tamanho médio de partícula de 30 a 250nm. A isoterma de adsorção-desorção de nitrogênio determinou uma área de superfície específica média de 280,38m²/g. IFTR, XRF, SPECMIN-TSG mostraram espectros com a presença de minerais de vermiculita, alofano e bentonita. Com TGA/DCS, foi observada uma perda de massa de até 42,5% para as argilas A1, A2, A3, na temperatura final de calcinação de

1000°C, com manifestações endotérmicas e exotérmicas. A alta capacidade de adsorção foi encontrada para as argilas A1 e A2, acima de 30% em sua ordem e acima dos outros estratos geológicos; a propriedade foi ativada quando a argila foi calcinada na janela de temperatura de 250 a 300°C. A espectroscopia de dispersão de energia (EDS) confirmou a presença de Si e Al na amostra de mistura betuminosa melhorada com aditivo A1. A SEM confirmou a presença de aditivo A1 esfoliado e disperso na mistura betuminosa melhorada preparada com 3% em peso de agente ativo. No DSR (T= 70°C operacional), o módulo complexo $G^* = 2326\text{pa}$ (640pa original) e $\delta = -8,7^\circ$ pontos (84° original) foram medidos, com uma melhoria de 363%. O novo material é aplicável como pavimento de estrada em áreas de temperatura ambiente média e alta devido à sua maior rigidez.

according to their layers (1:1, 2:1 and 2:1:1:1) based on the number and arrangement of tetrahedral and octahedral layers in their basic structure. There is a subdivision into five groups (mica, kaolinite, chlorite, vermiculite, smectite and amorphous) whose difference is their net charge. The present study is based on the use of smectite, which groups the phyllosilicate mineral species, the most important of which are montmorillonite, nontronite, beidellite, hectorite, and

saponite (Barton and Karathanasis, 2012). Within the smectites there is montmorillonite, and it is a 2:1 phyllosilicate, which forms the basis or is the main component of bentonite clay and allophane. A derived material is bentonite and represents the chemical alteration of a vitreous material of igneous origin of volcanic origin present in pyroclastic flows and eruptions of lava and volatile ash particles (Anavatan *et al.*, 2023). Today, bentonite is an important

material for applications in the food and medicine industry (Astuti *et al.*, 2023), technology for paints (Bourgault *et al.*, 2023), in the pharmaceutical and cosmetics industries (Rana and Kim, 2024), as catalysts (Zahraoui *et al.*, 2023), wastewater treatment (Sanavada *et al.*, 2023), and as oil well drilling fluids (Quitian *et al.*, 2022). Global bentonite production has increased from 2017 to 2021 from 1.83 to 1.92x10⁷ metric tons according to the British Geological Survey

report (Idoine *et al.*, 2023). According to SGM - Agency for Regulation and Control of Energy and Non-Renewable Natural Resources (Agencia de Regulación y Control de Energía y Recursos Naturales No Renovables), Ecuador's exploitation of bentonite is marginal among non-metallic materials. The main deposits of the mineral are Dos Bocas Member of the Tosagua Formation, of Miocene age, located in the coastal region of Ecuador, in the Santa Elena

canton (9°739.190N - 556.783E). The company "NUTRIB S.A" industrializes calcium bentonite for production of agricultural fertilizer (100% organic) (Campos and Hidalgo, 2014). Upper member of the Azogues Group of Miocene to Pliocene age, located in the Azogues-Cuenca sedimentary basin, towards the eastern flank of the Azogues province syncline, in the site called Loma Blanca (9°695.500N 740.200E), that is a bentonite clay deposit in the form of a lens intercalated between lamellar siliceous shales; the thickness of the stratum ranges from 0.5 to 7.0m. Proven reserves as of November 1986 were of the order of 500,000 tons and probable reserves of 108,000tons. San Cayetano Formation located in the Miocene sedimentary basins of Loja and Malacatos-Catamayo, smectite clays occur (Cornejo, 2017). In province of Santo Domingo de Tsáchilas, to 120km south of Quito, there are important accumulations of weathered clay materials, they constitute the San Tadeo geological formation (9°973.763N 695.779E, Figure 1a, elevation 443m ASL), in an area greater than 4000km² (Kaufhold *et al.*, 2009). The samples studied from the Dos Bocas location of the Tosagua Formation were estimated between 15.3% and 25.6% of the smectite minerals in the clays, however, bentonites from other deposits have been little studied and their commercial exploitation has been focused on additives for animal concentrates and pottery. Bentonite is abundant and inexpensive, with high cation exchange properties, which makes it a candidate adsorbent for the removal of heavy metals from wastewater or for integration with other materials (Liu *et al.*, 2023). The use of cationic surfactants in the chemical modification of clay minerals to generate organoclays (He *et al.*, 2006) can be used in remediation or modification of polymers (Archibong *et al.*, 2023). In addition, its properties of adsorption of many products make it a

potential alternative for combining it with other materials (Iftikhar *et al.*, 2023; Monteiro *et al.*, 2023; Yousif *et al.*, 2024). In the present study, the clay of the Tadeo Formation was characterized physically, chemically, and mineralogically, and its potential and use for the preparation of clay additives for HMA hot bitumen mixes was evaluated, and the rheological parameters of complex modulus G^* and phase angle δ were improved. This new material could be used in roads in temperate and warm zones.

Materials and Methods

Bulk clay collection

Samples were taken from the different geological horizons (Figure 1a) of the San Tadeo formation, using the Panel method. The basic equipment needed for rock sampling was a map of the region, a compass, a hammer, a magnifying glass, a pocketknife, acid (10% HCl), an indelible marker pen, nylon bags, a notebook, a ruler, gloves, safety glasses, a 12 lb. hammer, 20cm long chisels and boxes for safe transport of the samples. The collected samples (10kg) were stored in properly labeled containers. On the slope of the San Pedro de Chila road, samples were taken below the weathered zone of variable thickness between 1 and 3m, sampling depths were: sample A1 at 1m, sample A2

at 3m, sample A3 at 4.5m, sample A4 at 6m, sample A5 at 11m, and sample A6 at 16m. The upper levels were those of greatest geological interest for this investigation, according to previous studies (Kaufhold *et al.*, 2010). The obtained samples were dried at 105°C until reaching a constant weight, then mechanically crushed, pulverized in a ball mill, and sieved with 150 mesh (100 μ m) mesh. Representative bulk samples (1kg) of clays from levels A1 to A6 were worked. For microscopy and radiology, A1 and A2 (more superficial layers) were chosen and coincide with the studied levels PM4-1 and PM4-2 of the scientific paper by Kaufhold 2009. These levels contain allophane (> 60%) of better quality with SiO₂ contents of 41.5, 30.1% and Al₂O₃ of 22.7, 24.9%. The specific surface area of these clays was greater than 280m²/g. A1 was the clay selected and studied in more detail in this work because of its better aluminosilicate content.

Separation of the clay fraction

Fifty grams of the pulverized sample was suspended in 5 L of distilled water (pH of the solution was 6.8). It was disaggregated for approximately 25min with a magnetic stirrer and transferred to a graduated cylinder for gravity sedimentation according to Stokes' law (Cheng and Schachman, 1955). To obtain the fraction

below 2 μ m, the suspension was allowed to settle for 20h and the first 20cm of the suspension was removed. Subsequently, the suspension was centrifuged at 4500rpm for 15min to recover the clay fraction, which was dried at 105°C, ground and sieved at 150mesh. This sample was used for mineralogical analysis. The clay fraction can also be referred to as pure clay. It should be clarified that samples treated with NaOH (marked with *) and NH₃ (marked with **) were only evaluated with FTIR and SpecMin/TSG, as indicated in Table I. The treatment consists of aqueous solutions of 5M (molar) concentration, to remove impurities, carbonaceous matter, and washes until a pH value between 6.7 and 7.1 is obtained. The colloidal mass of the supernatant was dried at 105°C for a period of 12h (Norrfors *et al.*, 2015).

Mineralogical and chemical characterization of the clay

The clay sample (A1 and A2) was analyzed as random powder from the bulk material and as oriented assemblies of the <2 μ m fraction using a LabD8 ADVANCE (Boullé, 2017), at 40kV and 40mA, Cu K α radiation source (λ = 1.5418). The diffraction angle 2θ was scanned from 2° to 65° at a rate of 2°/min and a step size of 0.05°. Bragg's law was used to calculate the distance

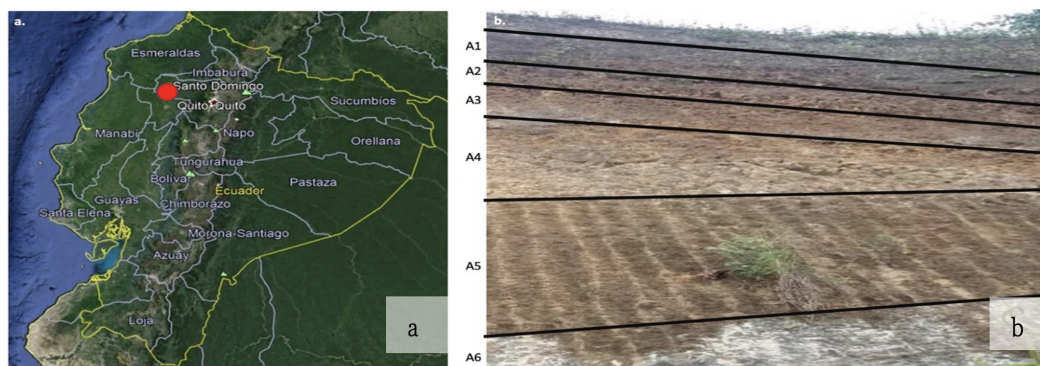


Figure 1. a) Geographical location and b) stratigraphic section of the San Tadeo Formation, with clay levels A1-A6.

TABLE I
PHYSICAL AND CHEMICAL LABORATORY TREATMENT AND ANALYSIS OF
SAMPLES A1-A6

Treatments	A1	A2	A3	A4	A5	A6
Pure sample	x	x	x	x	x	x
NaOH	x*					
NH ₃		x**				
Analysis						
Laser granulometry	x					
XRD, SEM	x	x				
FRX	x	x	x			
BET Isotherm	x					
SécMin/TSG, FTIR	x*	x**				
TGA, DSC, Adsorption	x	x	x	x	x	x
HMA integration	x	x	x	x	x	x

*: Clay treated with NaOH; **: Clay treated with NH₃.

between the silicate layers (Mena *et al.*, 2007). The XRD pattern was compared with the reference X-ray patterns for the identification of the different minerals using the X Pert High Score Plus software.

The chemical analyses were carried out by X-ray fluorescence using a S8 Tiger X-ray machine (XRF), with samples A1 and A2, dried at 105°C, and ground in an agate mortar until obtaining a grain size of less than <5µm on average, and 40mg of sample were mixed with 100mg of boric acid in the container, until having a totally homogeneous material, used to make briquettes of the mineral at 30mg/cm², and with the appropriate pressure, and it was verified that the surface is isotropic, which allowed making correct measurements. This technique was chosen since preliminary studies showed that the grain size of the sample is a critical factor affecting XRF results (Prandel *et al.*, 2012).

Fourier transform infrared spectrometry (FTIR) was performed with a VERTEX 70 instrument, which has a spectral range of 10000 to 400cm⁻¹. The records were from pure samples, plus A1* and A2**, pressed in granules with KBr powder at a nominal temperature of 105°C (Vaculíková *et al.*, 2018).

Using ZEISS Ultra 55 (SEM-EDS) equipment, A1 or A2

clay samples were placed on a rotating stage about the Cartesian x, y and z axes in the vacuum chamber of the scanning electron microscope. The heated tungsten filament generated and accelerated electrons at a constant emission flux of 100µA and varying voltages from 15 to 30kV. It was operated at magnifications of 100 × up to 25000 (Capasso and Yamaguchi, 2024).

The nitrogen adsorption-desorption isotherm of the clay fraction was determined with Multi-Point BET equipment at 77°K after degassing sample A1 (0.05 g) for 1h at 90°C followed by 3h at 400°C under vacuum. The specific surface area (SBET) was measured using the BET equation and the total pore volume was evaluated for nitrogen adsorption at a relative pressure of 0.99. The microporous specific surface area and microporous volume were calculated by the Harking-Jura equation (Anouar *et al.*, 2019) (Amin *et al.*, 2015).

The particle diameter and size distribution of sample A1 (0.025 g) were obtained with the LA-950 V laser scattering particle size distribution analyzer. The clay was previously dehydrated at 105°C. The nanometer particles tend to rise towards the top of the calcination chamber, and the heavier ones accumulate at the bottom of the vessel; consequently, the

measurement was performed at three points of the vessel (Benedet *et al.*, 2024).

Spectral images of A1(pure) and NaOH and NH₃ treated samples were obtained with HyLogger3 (SpecMin/TSG) and compared with the patterns of the mineral libraries of the samples. The deviation intervals of the curves and their specific depths were determined. Thus, the clays evaluated corresponded to different patterns (Liu *et al.*, 2014).

The thermogravimetric analysis of samples A1 to A6 was performed with the SDT Q 600 Netzsch equipment, with an air flow of 75cm³/min and a heating rate of 10°C/min, in the range of 100 to 1000°C. On the other hand, the thermal differentials of the same samples were recorded with the DSC-TGA as a function of time (Poussardin *et al.*, 2024).

Atmospheric adsorption tests for samples A1 to A6 were obtained with the BOECO-Germany-Instruments high-precision balance system (sensitivity of 0.001g). Thirty mg of each clay was calcined to 325°C with a rising temperature gradient of 10°C/min. It was then allowed to stand at one atmosphere pressure and 80% humidity. Mass increment measurements were carried out every 5min until 2500 min (Brunauer *et al.*, 1938), (Kausar *et al.*, 2018), (Yariv and Lapidés, 2000).

For the application of clay utilization, it was chosen the controlled calcination (250 to 300°C) of the clay, then milled in a ball mill (20min), sieved at 150 mesh, and transformed into an additive for the HMA hot bitumen mix. It was mixed at 4500rpm and 160°C with the AD500S-H - homogenizer disperser mixer at times of 30, 60, 90 and 120 minutes. The measurement of rheological parameters and stiffness increase of the HMA samples were measured with Dynamic Shear Rheometers (DSR 81-PV6202) (Maharaj, 2023). Perform the critical rheological characterization analysis required for Super Pave PG classification of asphalt binders, according to the values found for Complex Modulus G* and Phase Angle δ. The DSR test uses a thin sample of asphalt binder placed between two circular plates. The lower plate is fixed while the upper plate oscillates back and forth across the sample to create a shearing action. The Model 81-PV6202 DSR performs superpave performance classification per AASHTO T315 and ASTM D7175, asphalt binder viscosity determination per AASHTO T316 and ASTM D4402. Asphalt binder bitumen is viscoelastic. This means that they behave partly as an elastic solid (deformation due to loading is recoverable, i.e., it can return to its original shape after the load is removed) and partly as a viscous liquid (deformation due to loading is not recoverable, i.e., it cannot return to its original shape after the load is removed). DSR can quantify both elastic and viscous properties. This makes it well suited for characterizing bitumen over the in-service pavement temperature range. The more viscous the material is, the greater the phase angle will be. The limiting values of the phase angle are: 1. Purely elastic material: δ= 0 degrees and 2. Purely viscous material: δ= 90 degrees. The specified DSR oscillation rate of 10 radians/second is intended to simulate the shear action corresponding to a traffic speed of

approximately 90km/hr. G^* and δ are used as predictors of rutting and fatigue cracking of the HMA. Early in the pavement life, rutting is the primary concern, while later in the pavement life, fatigue cracking becomes the primary concern (Iskender, 2016; Sedaghat *et al.*, 2020).

Results and Discussion

Mineralogical characterization of the clays A1 and A2

In clay A1, the peak intensity $2\theta = 26.55^\circ$ indicates the presence of quartz and siliceous elements; allophane has quartz mixed at $2\theta = 28.15^\circ$ and 18.65° with non-crystalline material. Low peaks with angles of $2\theta = 10.58^\circ$ correspond to actinolite and, at values of $2\theta = 5.0^\circ$, to montmorillonite (bentonite) Figure 2a. In sample A2 it is observed that the peak intensity $2\theta = 26.57^\circ$ indicates the presence of quartz and silica elements, and the allophane has quartz mixed at $2\theta = 30.48^\circ$ and 21.02° with non-crystalline material. Low peaks at angles of $2\theta = 12.16^\circ$ correspond to actinolite and at values of $2\theta = 5.0^\circ$ to montmorillonite Figure 2b. The mineralogy of the two clays bears similarity of sedimentary volcanic bodies.

Spectral images of samples A1 (pure) and those treated with NaOH and NH_3 were obtained with SpecMin/TSG equipment and compared with the patterns of the mineral Allophane (AlloJP2f.002) and Bentonite. As for the absorption characteristics of the untreated sample, they coincide in wavelength and absorption depth with the allophane standard sample and present a similarity of 90% (Figure 3a). The second case matches the bentonite spectrum (Figure 3b) with a similarity of 73%. The spectra of the treated sediment samples, a) A1 + NH_3 and b) A1 + NaOH, partially coincide in depth (1400 and 1910nm) with allophane, bentonites and smectites, due to the affectation of the chemical treatment

performed (Percival *et al.*, 2018).

Physicochemical characterization of treated and pure A1 and A2 clays

The chemical composition of the A1 clay is shown in Figures 4a (NaOH treated) and 4b (pure). In (a) the values of the depressed peaks were found to be 3249.66, 1585.54,

1280.39, 918.20, 791.30, and 603.95cm^{-1} . The interpretation indicated that the value of 3249.66cm^{-1} corresponds to the possibility of the existence of OH groups in the Si-OH and Al-OH structures. The value of 1585.54cm^{-1} turned out to be deeper due to the treatment of the sample with H_2O_2 , showing the existence of OH groups within the molecules of the structure. At 1280.39cm^{-1} it

showed the manifestation of typical vibrations of OH-Al bonds. The peaks 918.20 , 899.26 , and 791.30cm^{-1} , are the result of energy absorption of Si-O-Si, Si-OH-Al, and Si-O-Al molecules in the frame of the respective FTIR spectra of the A1+NaOH and pure samples. Likewise, the chemical composition of A2 clay is shown in Figures 5a (treated with NH_3) and 5b (pure). In (a)

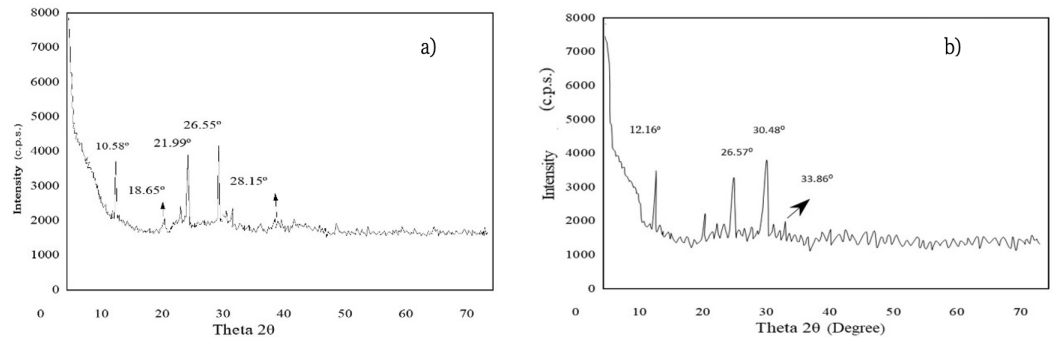


Figure 2. Powder X-ray diffractogram of a) A1 and b) A2 clays of the Tadeo Formation.

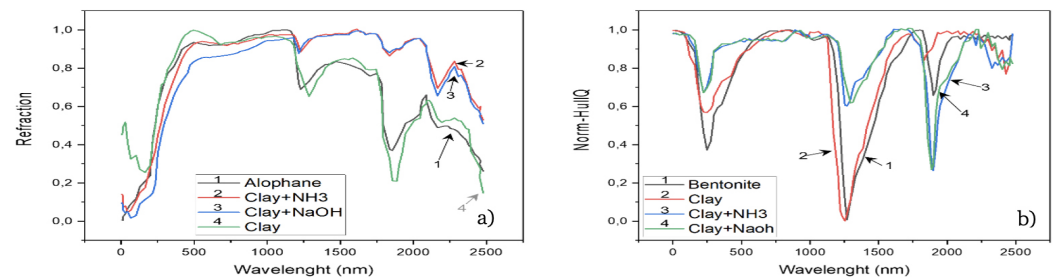


Figure 3. a) Spectra of A1 (pure) A1+ NaOH compared with spectra of allophane and b) Spectra of A1 (pure) and A1+ NH_3 compared with spectra of bentonite/smectite from Montana, Nevada (USA).

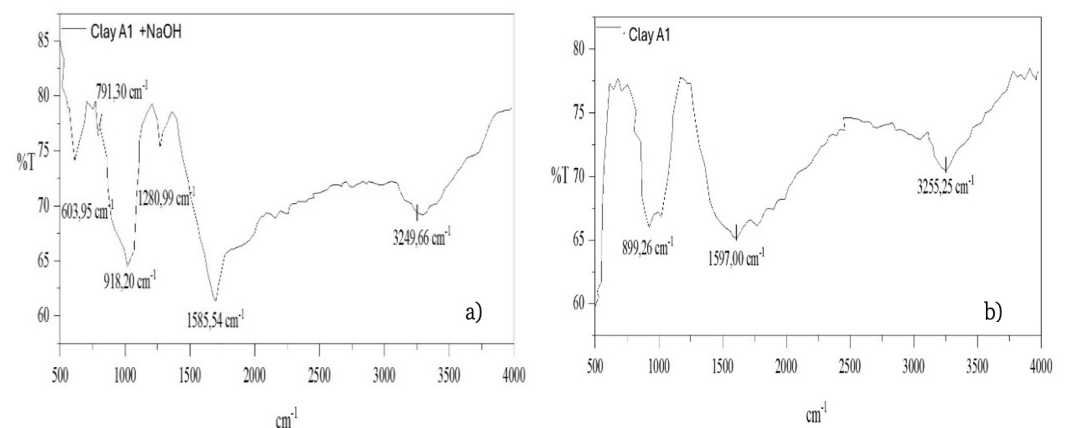


Figure 4. FTIR spectra of clay A1 a) treated with NaOH and b) pure.

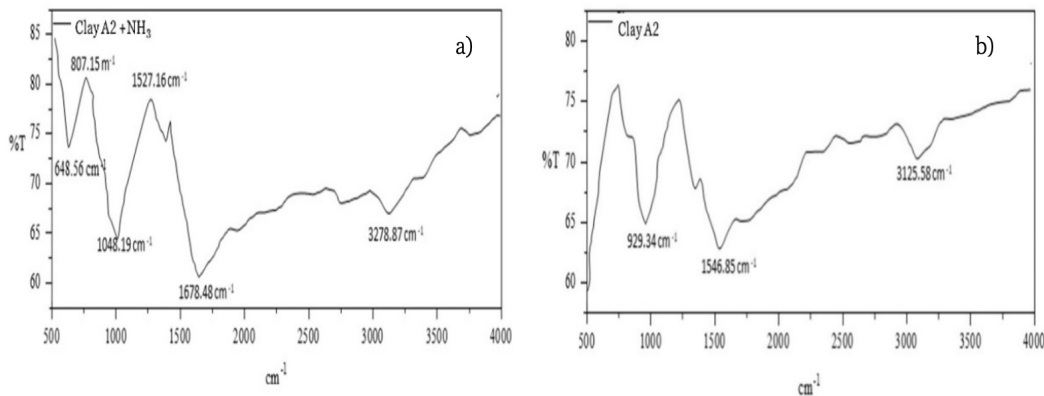


Figure 5. FTIR spectra of clay A2 a) treated with NH₃ and b) pure.

the values of the depressed peaks were found to be 3278.87, 1678.48, 1527.16, 1048.19, 807.15 and 648.56 cm⁻¹. The interpretation indicated that the value of 3278.87 cm⁻¹ corresponds to the possible existence in OH groups of Si-OH and Al-OH structures. The value of 1678.48 cm⁻¹ corresponds to OH groups within the molecules of the structure, and NH₃ does not significantly modify the functional groups. The value 1527.16 cm⁻¹ showed the manifestation of typical vibrations of OH-Al bonds. The peaks 1048.19, 807.15 and 648.56 cm⁻¹ are the result of energy absorption of Si-O-Si, Si-OH-Al and Si-O-Al molecules within the octahedron framework. In sample (b), depressed peaks were found as in sample A1 at 3125.58, 1546.85 and 929.34 cm⁻¹; the value at 3125.58 cm⁻¹ showed the existence of Al-OH and Gibbsite groups constituting the allophane planes. At 1546.85 cm⁻¹ the existence of OH radicals belonging to the octahedral structures of lamellar A1 was demonstrated. At 929.34 cm⁻¹ the existence of Si and Al, Si-O-Si and Si-OH-Al structures was indicated. Values below 500 cm⁻¹ indicated the absence of volcanic ash, and it is a typical wall with a clay structure as (OH) Si (OAl)₃; the definition of each functional group is approximate (Ahmed *et al.*, 2018). The existence of Si, Al, Fe and OH functional groups, characteristic elements of volcanic clays, was evidenced.

TABLE II
RESULTS OF X-RAY FLUORESCENCE ANALYSIS OF CLAYS A1, A2 AND A3

Element	A1	A2	A3
Si	0.3077	0.3357	0.3246
Al	0.2987	0.3259	0.3151
Fe	0.1186	0.1294	0.1251
Na	0.0316	0.0344	0.0333
Ca	0.0138	0.015	0.0145
Ti	0.0116	0.0127	0.0123
Mg	0.0111	0.0121	0.0117
K	0.0041	0.0045	0.0043
Mn	0.0015	0.0017	0.0016
P	0.0013	0.0014	0.0014
S	0.001	0.0011	0.0011
TOC	0.199	0.126	0.155
Overall	1	1	1

A1: Clay level 1; A2: Clay level 2; A3: Clay level 3.

The functional groups of aluminosilicates with a Si/Al ratio of 1.6 (Kaufhold *et al.*, 2009). Table II shows the results of calcination at 956°C of 3 samples of the level material (A1, A2 and A3). Chemical analysis was carried out with XRF, where the highest fraction of atoms was found to be Si and Al with respect to unity; the other fractions in smaller magnitudes were found to be of the chemical elements Fe, Na, Ca, Ti, Mg, K, Mn, P, and S (Alorabi *et al.*, 2021). In addition, BET assays were performed and the adsorption and desorption isotherms of the activity between the clay (A1) and an N₂ moiety were presented. There are two distinctive features of the N₂ type loop thus, first

the adsorption resembles a type II isotherm and second the lower boundary of the desorption branch is usually located at the

cavitation-induced p/p₀. The loop of this type is given by non-rigid aggregates of particles in the form of a plate (Garvie *et al.*, 2024). The specific surface area averaged 280.38 m²/g. The pore volume at p/p₀ = 0.99 is 60 cm³/g STP. In the t plot method was used to determine the specific area and the volume developed by the micropores of the samples. These values are at p/p₀ = 0.0123 and 14.6 cm³/g STP per g for the clay fraction Figure 6.

The Laser Granulometry technique allowed us to know the diameter of the A1 clay particles and their size distribution. The 71.2% of the

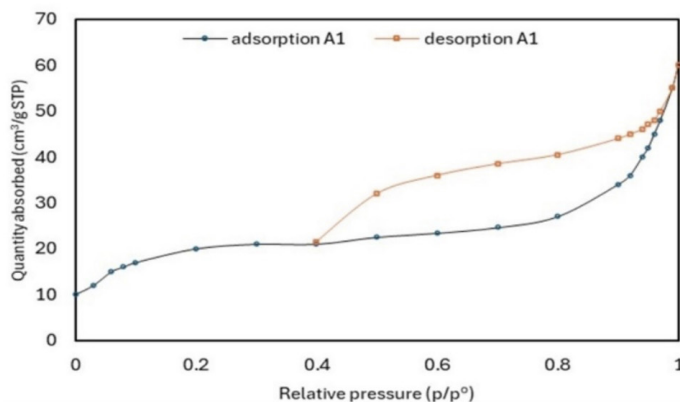


Figure 6. N₂ physisorption isotherm of pure A1 clay.

particles had a maximum diameter of 200nm, 43.3% reached 100nm, and the total number of particles did not exceed 250nm (it has micro and meso porosity) and the results are shown in Table III (Dur *et al.*, 2004).

Thermogravimetry and adsorption of clays A1 to A6

Figure 7a shows the TGA test results for clay samples A1 to A6, the TGA measured the mass loss due to the volatilization of certain constituent elements of oxygen, hydrogen, and carbon when the temperature gradually increased up to 1000°C, likewise the DCS showed the behavior of endothermic and exothermic changes, which resulted in an oscillatory behavior Figure 7b. Table IV shows the results of calcination up to Tf= 1000°C, of clays A1 to A6, where the highest losses were verified for A1, A2 and A3 with values of 42.5%, 40.3% and 34.9% respectively, in addition the initial temperature (To M loss) of mass loss (%M loss) of each sample is presented. Table V shows the results of the oscillatory behavior of the exothermic and endothermic changes with respect to temperature (ΔT) and percent mass loss in the respective event.; the most important points observed were: (a) mass loss started at the temperature of 178°C under endothermic conditions; (b) between 380°C and 555°C the removal of organic matter and hydroxyl (OH) was corroborated; (c) at 956°C spicules were formed in a process of diagenesis of the mineral under exothermic conditions. Samples A1, A2 and

A5 had 3 thermal change events in the calcination span up to 1000°C (Kök *et al.*, 2021). The atmospheric adsorption test BET (Brunauer *et al.*,1938), was carried out at all 6 levels (A1 a A6). The calcination temperature was controlled, allowed to rest in air and the equipment measured the results shown in Figure 8. In the test, it was observed that samples A1 and A2 achieved higher mass gloating capacity corresponding to 1.89mg and 1.8mg respectively, in a resting time of 2500 seconds after calcination 325°C. At higher temperatures, 475°C, the texture of the clays changed, which involved the destruction of the pillars (Na⁺, Fe²⁺, Mg²⁺ and Li⁺ ions) of the structures (Si-Al-Si). The samples of layers A4 and A5, presented a low adsorption rate (Ramezanipour *et al.*, 2021).

Chemical evaluation of bituminous mixtures with clay additive

The SEM/EDS energy dispersive spectroscopy

TABLE III
LASER GRANULOMETRY ANALYSIS DATA OF PURE A1 CLAY

Number	Particle Diameter (μ)	Retaines (%)	Past Accumulated
1	0.1	0.1	0.1
2	0.1	0.4	0.6
3	0.1	1.7	2.3
4	0.1	5.5	7.8
5	0.1	12.6	20.4
6	0.1	22.8	43.3
7	0.2	27.9	71.2
8	0.2	19.7	90.9
9	0.2	7.5	98.3
10	0.2	1.5	99.8
11	0.3	0.2	100

TABLE IV
MASS LOSS DATA WHEN SAMPLES OF CLAYS A1 TO A6 WERE CALCINED AT 1000°C

	To (°C)	Tf (°C)	M loss (%)
A1	178	1000	42.50
A2	212	1000	34.90
A3	192	1000	40.30
A4	213	1000	21.60
A5	167	1000	23.70
A6	258	1000	16.60

To: Mass loss onset temperature; Tf: Final calcination temperature.

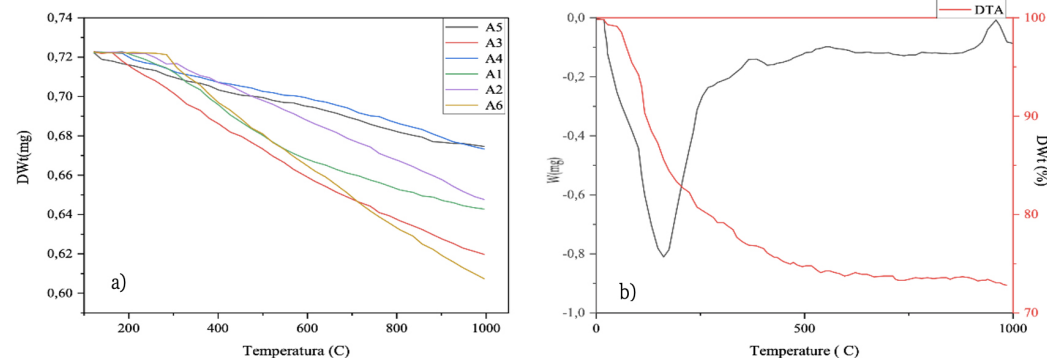


Figure 7. (a) TGA curves of clay samples A1-A6; (b) Thermogram of clay A1.

TABLE V
RESULTS OF THE OSCILLATORY BEHAVIOR OF THE EXOTHERMIC AND ENDOTHERMIC CHANGES WITH RESPECT TO TEMPERATURE (ΔT)(°C) AND PERCENT MASS LOSS (Δm)(mg)

A1		A2		A3		A4		A5		A6	
ΔT	$\Delta m(\%)$										
328	13.20	339	5.40	238	4.00	282	2.20	347	6.50	302	1.50
544	29.80	578	16.90	682	30.70	416	6.00	701	15.90	697	10.90
656	36.80	800	28.10			654	11.60	871	23.30		
723	39.20										

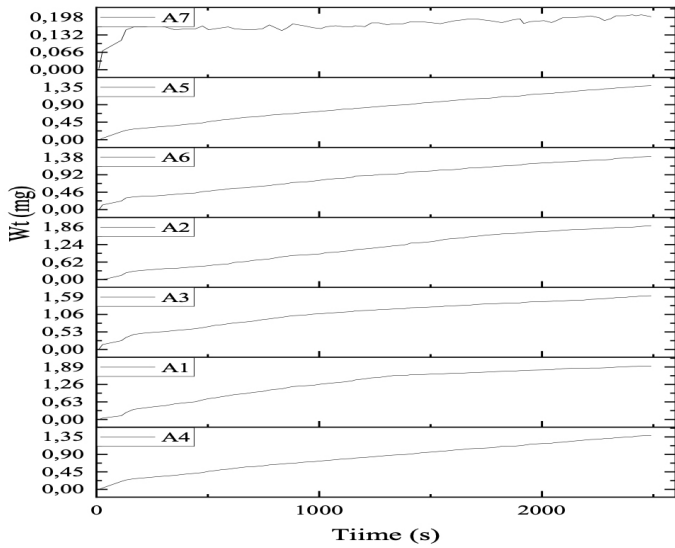


Figure 8. Absorption and weight gain profiles as a function of time for clays A1 to A6. A7 representing A1 calcined at 1000°C was included.

technique was used to evaluate the samples of asphalt bituminous mixtures with clay A additives. Figures 9a, b and

c, show Al and bitumen with the presence of Al, Si for clay and C for bitumen respectively. In Figure 9c, which represents the mixture of the two previous materials, the presence of the 3 preceding products and the potentials of 0.5, 1.52 and 1.81KeV can be seen. The presence of the chemical element's carbon, aluminum, and silicon as preponderant atoms in the materials investigated and shown in Figures 10a, c, e. On the other hand, the bituminous mixture with the clay additive A1 was observed, correctly finding the presence of the elements Al and Si dispersed in the bitumen matrix with C and can be seen in Figures 10d, f and b, respectively. The mixture corresponded to a concentration of 3% of the additive by weight (Theiss *et al.*, 2015).

Evaluation of the complex modulus and phase angle of bituminous mixtures and clay additive

To evaluate the efficiency of the asphalt mixes, we measure the grade performance PG= 70 which means taking the reading of G^* and δ of the DSR (test temperature 70°C), of the sample that has been placed in the parallel sticks of the equipment. If the value of G^* is equal to or greater than 1Kpa (thousand pascals) it is verified to have PG= 70. The value of δ can decrease, maintain, or increase in reference to the original bitumen before mixing. The optimum we look for in the mixtures with the clay additive, that the G^* increases and δ decreases with respect to the original bitumen that has 640 pa and of phase angle

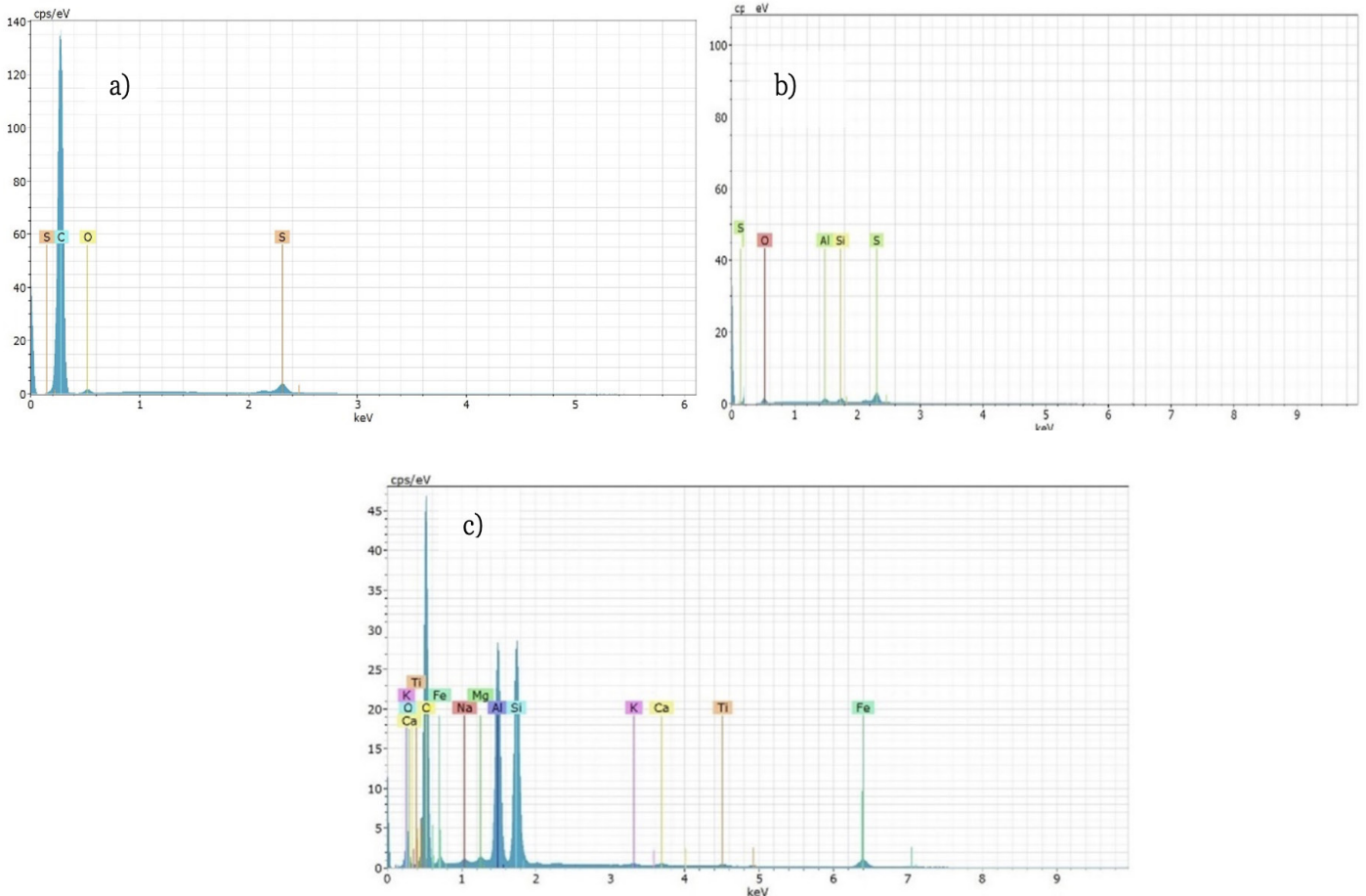


Figure 9. EDS diffractogram of a) sample of bitumen with presence of C, b) sample of clay with presence of Si and Al, c) sample of improved mixture of bitumen with clay additive of Si and Al.

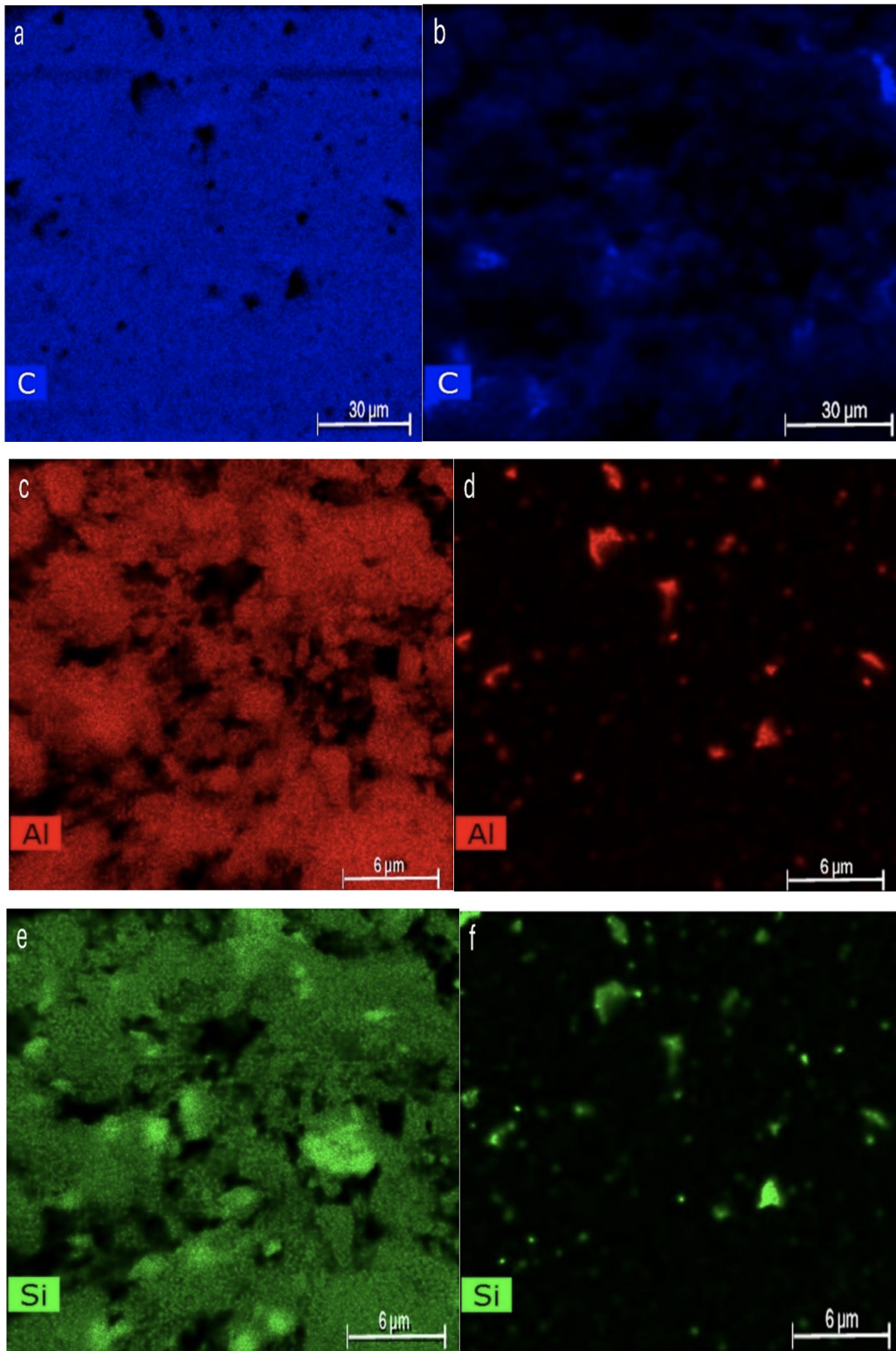


Figure 10. Presence of the chemical element's a) bitumen mixture with A1 additive and presence of Si Al, b) clay with negligible presence of C, c) A1 clay with abundance of Al, d) bitumen mixture with presence of Al, e) clay with abundance of Si and f) bitumen mixture with presence of Si.

84° as can be verified in Figures 11a y b at the point of T= 70°C. The mixtures that

exceeded PG (G*; δ) =70 are those that carried the A1, A2 and A3 clay additives with

values of (2326;75.63), (1821;76.5) and (1095;79.02) respectively, but above all the

A1 clay is the one that stands out for this application exceeding the reference level (1000 pa= 1Kpa) by 1686 additional points (mixing time 120min) Table VI.

Conclusions

Ecuador has an area of 4000km² of volcanic clay resource established in the San Tadeo geological formation, which has 6 strata from A1 to A6. In the physicochemical studies carried out on samples taken in the field, indicated the presence of more than 60% of aluminum and silicon compounds for levels A1 and A2. Laser granulometry measured particle size between 30 and 250 nm. Isothermal BET found that the specific surface area was 280.38m²/g. IFTR, XRF, SPECMIN-TSG spectrally evaluated the original samples and showed the presence of vermiculite, allophane and bentonite minerals. With TGA/DCS a mass loss of up to 40% was observed for clays A1, A2 and A3, when the samples were calcined at 1000°C with various endothermic and exothermic manifestations. Adsorption capacity indicated that A1 and A2 showed 30% higher than the others, and the property was activated when the clay was calcined in the temperature window of 250 and 300°C. The EDS diffractogram indicated the presence of Si and Al in the sample of bitumen blend enhanced with additive A1, and the images (SEM) confirm the presence of the exfoliated and dispersed additive prepared with 30% by weight of active agent. The positive rheological parameters measured with DSR (T= 70°C) of the bituminous mixtures with A1 clay additive, complex modulus G* and phase angle δ, show that the new additive modified G* to 2326pa (original 640 pa) and δ decreased by -8.7 original points), with an improvement of 363%. The new bituminous binder will be suitable for road pavements in medium and warm temperature zones due to its improved stiffness.

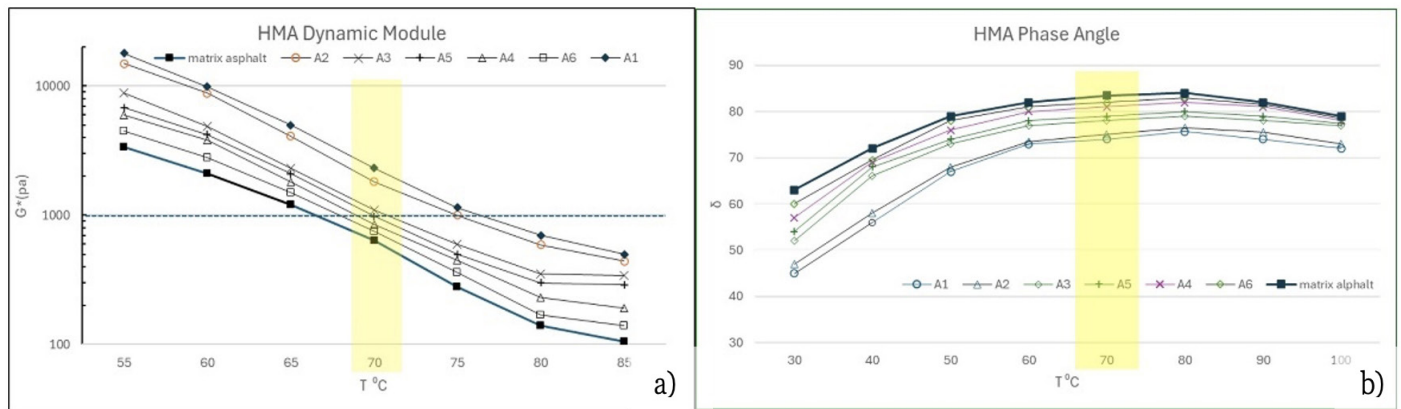


Figure 11. Results in yellow zone of positive rheological parameters ($T= 70^{\circ}\text{C}$) of bitumen mixtures with clay additive of A1, A2: a) Complex Modulus G^* and b) phase angle δ .

TABLE VI
POSITIVE ADDITIVE RESULTS FOR A1 AND A2 CLAYS OF THE SIX TYPES, AS MEASURED BY G^* AND δ PARAMETERS IN MIXES WITH BASE BITUMEN. A7 INDICATES THE ORIGINAL BASE BITUMEN

Clay	T ($^{\circ}\text{C}$)	G^* (pa)	δ ($^{\circ}$)
A1	70	2326	75.63
A2	70	1821	76.5
A3	70	1095	79.02
A4	70	982	80.1
A5	70	858	82.3
A6	70	759	83.9
A7	70	640	84

REFERENCES

- Ahmed A, Chaker Y, Belarbi H, Abbas O, Chotard N, Abassi B, Van Nhien N, El Hadri M, Bresson S (2018) XRD and ATR/FTIR investigations of various montmorillonite clays modified by monocationic and dicationic imidazolium ionic liquids. *Journal of Molecular Structure* 1173: 653–664. <https://doi.org/10.1016/J.MOLSTRUC.2018.07.039>
- Alorabi Q, Hassan S, Alam M, Zabin A, Alsenani I, Baghdadi E (2021) Natural Clay as a Low-Cost Adsorbent for Crystal Violet Dye Removal and Antimicrobial Activity. *Nanomaterials* 11: 2789. <https://doi.org/10.3390/NANO11112789>
- Amin T, Alazba A, Shafiq M (2015) Adsorptive Removal of Reactive Black 5 from Wastewater Using Bentonite Clay: Isotherms, Kinetics and Thermodynamics. *Sustainability* 7: 15302–15318. <https://doi.org/10.3390/SU71115302>
- Anavatan E, Ant Bursali E, Yurdakoç M (2023) Synthesis and characterization of bentonite based zinc complexes. *Journal of Sustainable Construction Materials and Technologies* 8: 112–119. <https://doi.org/10.47481/JSCMT.1272416>
- Anouar F, Elmchaouri A, Taoufik N, Rakhila Y (2019) Investigation of the ion exchange effect on surface properties and porous structure of clay: Application of ascorbic acid adsorption. *Journal of Environmental Chemical Engineering* 7: 103404. <https://doi.org/10.1016/J.JECE.2019.103404>
- Archibong N, Orakwe C, Ogah A, Mbam O, Ajah A, Okechukwu E, Igberi O, Okafor J, Chima O, Ikelle I (2023) Emerging progress in montmorillonite rubber/polymer nanocomposites: a review. *Journal of Materials Science* 58: 62396–2429. <https://doi.org/10.1007/S10853-023-08173-4>
- Astuti A, Mawardi K, Darini M, Sastrohartono K, Anam M (2023) The Effect of Nanobentonite Supplementation on Reducing the Toxicity of Aflatoxin B1. In Kampung Unggul Balitbangtan Chickens Diet. *Journal of World's Poultry Research*. <https://doi.org/10.36380/JWPR.2023.27>
- Barton CD, Karathanasis AD (2002) Clay Minerals. In: Lal R, Ed., *Encyclopedia of Soil Science*. CRC Press. New York, USA, pp. 187-192.
- Benedet A, Zaccaron A, Inocente M, de Souza Nandi V, Arcaro S, Raupp F, Gorini D (2024) Development of eco-friendly clay ceramics using rice husk ash as a secondary mineral source of quartz. *Materials Today Communications* 38: 108103. <https://doi.org/10.1016/J.MTCOMM.2024.108103>
- Bergaya F (2006) General Introduction: Clays, Clay Minerals, and Clay Science. Ed(s) Bergaya F, Theng BKG, Lagaly G. *Developments in Clay Science*. Elsevier, Vol. 1, pp. 1–18. <https://www.sciencedirect.com/science/article/pii/S1572435205010019>
- Boulle A (2017) DxTools: processing large data files recorded with the Bruker D8 diffractometer. *J. Appl. Cryst.* 50: 967–974. <https://doi.org/10.1107/S1600576717005192>
- Bourgault S, Wiley P, Farber A, Jacobs J (2023) Enabling Parametric Design for Clay 3D Printing Through an Action-Oriented Toolpath Programming System. *Conference on Human Factors in Computing Systems - Proceedings*. Hamburg, Germany, <https://doi.org/10.1145/3544548.3580745>
- Brigatti M, Galan E, Theng BKG (2013) Structure and mineralogy of clay minerals science. B. T.-D. in clay, & undefined. (n.d.) In Eds. Faiza Bergaya, Gerhard Lagaly. *Developments in Clay Science*. Elsevier. Vol. 5. pp: 2--81. <https://www.sciencedirect.com/science/article/pii/B978008098258800002X>. (Cons. 05/16/2024).
- Brunauer S, Emmett H, Teller E (1938) Adsorption of Gases in Multimolecular Layers. *Journal of the American Chemical Society* 60: 309–319. <https://doi.org/10.1021/JA01269A023>. A S S E T / J A 0 1 2 6 9 A 0 2 3 . F P . P N G _ V 0 3
- Capasso L, Yamaguchi A (2024) A batoid hembryo (Chondrichthyes: Batoidea), from the marine upper Cenomanian (Late Cretaceous) Sannine limestone of Hjoula, Lebanon. *Historical Biology* 36: 293–308. <https://doi.org/10.1080/08912963.2022.2162395>
- Cheng Y, Schachman K (1955) Studies on the validity of the Einstein viscosity law and Stokes' law of sedimentation. *Journal of Polymer Science* 16: 19–30. <https://doi.org/10.1002/POL.1955.120168102>
- Cornejo P (2017) Depósitos minerales no metálicos del Ecuador. Escuela Politécnica Nacional. Quito, Ecuador. 37 pp. <https://doi.org/10.13140/RG.2.2.24008.11523>.
- Campos A, Hidalgo M (2014) *Producción de Bentonita Industrial y Agrícola*. Tesis, Universidad de Guayaquil, Ecuador.

- Dur C, Elsass F, Chaplain V, Tessier D (2004) The relationship between particle-size distribution by laser granulometry and image analysis by transmission electron microscopy in a soil clay fraction. *European Journal of Soil Science* 55: 265–270. <https://doi.org/10.1111/J.1365-2389.2004.00597.X>
- Garvie J, Trif L, Cotto D, Asphaug E, Hoover G (2024) High surface area and interconnected nanoporosity of clay-rich astro-materials. *Scientific Reports* 14: 1–11. <https://doi.org/10.1038/s41598-024-61114-2>
- He H, Duchet J, Galy J, Gérard F (2006) Influence of cationic surfactant removal on the thermal stability of organoclays. *Journal of Colloid and Interface Science* 295: 202–208. <https://doi.org/10.1016/J.JCIS.2005.08.013>
- Ildoie N, Raycraft E, Price F, Hobbs S, Deady E (2023) World Mineral Production. *British Geological Survey 2017-2021*. London, UK. 88 pp. https://nora.nerc.ac.uk/id/eprint/534316/1/WMP_2017_2021_FINAL.pdf
- Iftikhar S, Shah M, Mir S (2023) Potential Application of Various Nanomaterials on the Performance of Asphalt Binders and Mixtures: A Comprehensive Review. *International Journal of Pavement Research and Technology* 16: 1439–1467. <https://doi.org/10.1007/S42947-022-00207-5>
- Iskender E (2016) Evaluation of mechanical properties of nano-clay modified asphalt mixtures. *Measurement* 93: 359–371. <https://doi.org/10.1016/J.MEASUREMENT.2016.07.045>
- Kaufhold S, Kaufhold A, Jahn R, Brito S, Dohrmann R, Hoffmann R, Gliemann H, Weidler P, Frechen M (2009) A new massive deposit of allophane raw material in Ecuador. *Clays and Clay Minerals* 57: 72–81. <https://doi.org/10.1346/CCMN.2009.0570107>
- Kaufhold S, Ufer K, Kaufhold A, Minerals S (2010) Quantification of allophane from Ecuador. *Clays and Clay Minerals* 58: 707–716. <https://doi.org/10.1346/CCMN.2010.0580509>
- Kausar A, Iqbal M, Javed A, Aftab K, Nazli iH, Bhatti HN, Nouren S (2018) Dyes adsorption using clay and modified clay: A Review. *Journal of Molecular Liquids* 256: 395–407. <https://doi.org/10.1016/J.MOLLIQ.2018.02.034>
- Kök V, Varfolomeev A, Nurgaliev K (2021) TGA and DSC investigation of different clay mineral effects on the combustion behavior and kinetics of crude oil from Kazan region, Russia. *Journal of Petroleum Science and Engineering* 200: 108364. <https://doi.org/10.1016/J.PETROL.2021.108364>
- Liu H, Fu T, Sarwar T, Yang H (2023) Recent progress in radionuclides adsorption by bentonite-based materials as ideal adsorbents and buffer/backfill materials. *Applied Clay Science* 232: 106796. <https://doi.org/10.1016/J.CLAY.2022.106796>
- Liu J, Yao Y, Wang Y, Yuan Z (2014) Infrared spectral identification of metasomatic alteration minerals and its implication to gold exploration in Shihu Gold Deposit, Hebei Province, P.R. China. *International Symposium on Optoelectronic Technology and Application 2014: Infrared Technology and Applications*. Proceedings 9300, 93001J. <https://doi.org/10.1117/12.2072162>
- Maharaj, R. (2023). The effect of the kaolinitic clay and asphaltenes on the rheological properties of Trinidad Lake Asphalt and Trinidad Petroleum Bitumen-clay composites / Rean Maharaj. <https://jsst.uitm.edu.my/index.php/jsst/article/view/40>
- Mena J, Sun R, Lopez T, Azamar A, Aguilar H, Dominguez I, Odriozola A, Quintana P (2007) Nitrate removal using natural clays modified by acid thermo-activation. *Applied Surface Science* 253: 5762–5766. <https://doi.org/10.1016/J.APSUSC.2006.12.103>
- Monteiro L, Baghaee T, Shafiee M, Hashemian L (2023) Investigating the Addition of Organomontmorillonite Nanoclay and Its Effects on the Performance of Asphalt Binder. *Journal of Materials in Civil Engineering* 35. <https://doi.org/10.1061/JMCEE7.MTENG-15035>
- Norrfors K, Bouby M, Heck S, Finck N, Marsac R, Schäfer T, Geckeis H, Wold S (2015) Montmorillonite colloids: I. Characterization and stability of dispersions with different size fractions. *Applied Clay Science* 114: 179–189. <https://doi.org/10.1016/J.CLAY.2015.05.028>
- Percival B, Bosman A, Potter G, Peter M, Laudadio B, Abraham C, Shiley A, Sherry C (2018) Customized spectral libraries for effective mineral exploration: Mining national mineral collections. *Clays and Clay Minerals* 66: 297–314. <https://doi.org/10.1346/CCMN.2018.064103>
- Poussardin V, Wilson W, Paris M, Tagnit A, Deneele D (2024) Calcined clays as supplementary cementitious materials: A comparison between palygorskite and kaolinite. *Construction and Building Materials* 416: 135180. <https://doi.org/10.1016/J.CONBUILDMAT.2024.135180>
- Prandel V, Saab C, Brinatti M, Giarola B, Leite C, Cassaro M (2012) Mineralogical analysis of clays in hardsetting soil horizons, by X-ray fluorescence and X-ray diffraction using Rietveld method. *The Journal for Radiation Physics, Radiation Chemistry and Radiation Processing* 95: 65–68. <https://doi.org/10.1016/j.radphyschem.2012.12.017>
- Punia S, Ilyas A, Chowdhury A, Navaf M, Sunooj V, Siroha K (2023) Bentonite clay as a nanofiller for food packaging applications. *Trends in Food Science & Technology* 142: 104242. <https://doi.org/10.1016/J.TIFS.2023.104242>
- Quitian H, Andrade V, Franco T (2022) Bentonite-free water-based drilling fluids at HP/HT condition: a rheometric analysis. *Rheologica Acta* 61: 841–855. <https://doi.org/10.1007/S00397-022-01356-X/FIGURES/14>
- Ramezanipour H, Ghaemi A, Godarziani H (2021) Eco-friendly CO₂ adsorbent by impregnation of diethanolamine in nanoclay montmorillonite. *Environmental Science and Pollution Research* 28: 55754–55770. <https://doi.org/10.1007/S11356-021-14920-4/METRICS>
- Rana S, Kim S (2024) Bentonite in Korea: A Resource and Research Focus for Biomedical and Cosmetic Industries. *Materials* 17: 1982. <https://doi.org/10.3390/MA17091982>
- Sanavada K, Shah M, Gandhi D, Unnarkat A, Vaghasiya P (2023) A systematic and comprehensive study of Eco-friendly bentonite clay application in esterification and wastewater treatment. *Environmental Nanotechnology, Monitoring & Management* 20: 100784. <https://doi.org/10.1016/J.ENMM.2023.100784>
- Sedaghat B, Taherian R, Hosseini SA, Mojtaba Mousavi S (2020) Rheological properties of bitumen containing nanoclay and organic warm-mix asphalt additives. *Construction and Building Materials* 243: 118092. <https://doi.org/10.1016/J.CONBUILDMAT.2020.118092>
- Theiss FL, López A, Scholz R, Frost RL (2015) A SEM, EDS and vibrational spectroscopic study of the clay mineral fraipontite. *Spectrochimica Acta Part A: Molecular and Biomolecular Spectroscopy* 147: 230–234. <https://doi.org/10.1016/J.SAA.2015.03.088>
- Vaculíková L, Plevová E, Ritz M (2018) Characterization of Montmorillonites by Infrared and Raman Spectroscopy for Preparation of Polymer-Clay Nanocomposites. *Journal of Nanoscience and Nanotechnology* 19: 2775–2781. <https://doi.org/10.1166/JNN.2019.15877>
- Yariv S, Lapidés I (2000) The effect of mechanochemical treatments on clay minerals and the mechanochemical adsorption of organic materials onto clay minerals. *Journal of Materials Synthesis and Processing* 8: 223–233. <https://doi.org/10.1023/A:1011320328102/METRICS>
- Yousif A, Zghair H, Alsaedi F (2024) Optimal design of mechanical performances of asphalt mixtures comprising nano-clay additives. *Open Engineering* 14: <https://doi.org/10.1515/ENG-2022-0586/HTML>
- Zahraoui M, Mokhtar A, Medjhouda K, Abdelkrim S, Boukoussa B, Djelad A, Hasnaoui A, Sassi M, Abboud M (2023) Catalytic Reduction of Congo Red to Low-Toxicity Forms Using a Low-Cost Catalyst Based on Modified Bentonite Material. *Clays and Clay Minerals* 71: 74–90. <https://doi.org/10.1007/S42860-023-00226-8>